Desalination and Water Treatment
www.deswater.com

doi: 10.5004/dwt.2018.22122

107 (2018) 182–194
March

Biosorption of Cd^{2+} and Zn^{2+} from aqueous solution using tilapia fish scale (Oreochromis sp): Kinetics, isothermal and thermodynamic study

Abideen Idowu Adeogun[a,*], Edwin Andrew Ofudje[a,b], Mopelola Abidemi Idowu[a]
Sarafadeen Olateju Kareem[c], Shappur Vahidhabanu, B. Ramesh Babu[d]

[a]*Department of Chemistry, Federal University of Agriculture, Abeokuta, Ogun State, Nigeria, Tel. +2348036126987, email: abuaisha2k3@yahoo.com (A.I. Adeogun)*
[b]*Department of Chemical Sciences, McPherson University, Sapade, Ogun State, Nigeria*
[c]*Department of Microbiology, Federal University of Agriculture, Abeokuta, Ogun State, Nigeria*
[d]*CSIR-Central Electro Chemical Research Institute, Pollution control division, Karaikudi- 630003, Tamil Nadu, India*

Received 28 December 2017; Accepted 26 February 2018

ABSTRACT

This work investigates the feasibility of removal of Cd^{2+} and Zn^{2+} from aqueous solution using a low cost biosorbent prepared from tilapia fish scale. Effects of some important parameters such as pH, initial metal concentrations, temperature and adsorbent dosage on adsorption process were investigated. The prepared biosorbent was characterized using scanning electron microscopy (SEM), transmission electron microscopy (TEM), energy dispersive X-ray analysis (EDAX), Fourier transform-infra red (FTIR), X-ray diffraction (XRD) and thermal gravimetry-differential thermal analysis (TG-DTA). Data from kinetic study were analyzed with pseudo-first-order, pseudo-second-order, Elovich and intra-particle diffusion models while equilibrium data were evaluated using Langmuir, Freundlich, Temkin and Dubinin–Radushkevich isotherm models. The adsorption kinetics of the metals ions followed pseudo-first-order with average rate constants of 4.95×10^{-2} and 3.89×10^{-2} min^{-1} for Cd^{2+} and Zn^{2+} respectively. Langmuir adsorption isotherm fitted the isotherm study with $R^2 > 0.9$ while the maximum adsorption capacities of 112.57 and 95.69 mg/g were obtained for Cd^{2+} and Zn^{2+} respectively. Negative values of ΔG^o obtained from thermodynamic evaluations revealed that the adsorption process is spontaneous. The values ΔH^o and ΔS^o obtained for Cd^{2+} and Zn^{2+} respectively are 13.06 and 14.61 kJ mol^{-1} and 43.0 and 48.64 J mol^{-1} K^{-1}. The results indicated that fish scale could be utilized as cheap, eco-friendly and excellent biosorbent for the removal of Cd^{2+} and Zn^{2+} from aqueous solution.

Keywords: Biosorption; Tilapia; Fish scale; Equilibrium; Kinetic; Thermodynamics

1. Introduction

Environmental contamination with toxic materials can be directly linked to rapid industrialization and urbanization as a result of discharge of industrial waste. Human activities including; mining, agriculture, transportation and industrial production processes release a high amount of heavy metals environment. Heavy metal pollution results primarily from burning of fossil fuels, smelting of ores, municipal wastes, fertilizers, pesticides and sewage [1]. Heavy metals contamination of environment is of great concern due to their ability to accumulate in the living tissues and their non-degradability, therefore, posing significant threat to human, animals and plants [2,3]. Cadmium has been listed as the sixth most poisonous substance endangering human health [4]. Exposure to fumes or dusts of cadmium metal or cadmium oxide may cause renal dysfunction, bone degeneration, lung insufficiency, liver damage, and hypertension [5], while chronic exposure through the respiratory tract produces a number of toxic effects, the most important of which is chronic emphysema, accompa-

*Corresponding author.

nied by renal disturbance [6]. Zinc is an essential element require for some biological activities, however, excess of zinc in living system is detrimental to health adverse effects of zinc intake could results in diarrhea, vomiting, nausea, abdominal cramps, loss of appetite, headache [7,8], while, chronic effects include damage to immune function, low copper status and neurological disorder [8,9]. It has been suggested that increase cadmium/zinc ratio is related to the occurrence of hypertension in man [6]. Thus, the removal of these heavy metals from contaminated wastewater before discharge into the environment becomes imperative. Various techniques have been developed for removal of pollutants from waste water, these include; coagulation, flocculation, chemical oxidation, membrane filtration, catalytic degradation, adsorption, and photochemical degradation [10,11]. However, ease of application and effectiveness for different types of pollutants are some of the advantages that favours the adsorption method when compared with all other methods. Biosorption is the use of adsorbent derived from living, inactive or non-living biomass, it emerged as an economic and eco-friendly option, a non-polluting process, easy to operate and highly efficient in treating wastewater containing low metal concentrations [12,13]. Biosorbent prepared from various natural materials had been used for heavy metal remediation of wastewater, these include Seashell, algae-yeast, jujube seed, peanut shell, palm shell, and Croaker fish scale [14–19].

This study exploits the availability of tilapia fish scales for preparation of biosorbent via calcination. The prepared biosorbent was characterized with XRD, FT-IR, SEM/EDAX, TEM, TGA/DTA and subsequently applied for the removal of Cd and Zn ions from aqueous solution in a batch process. Effects of various factors such as contact time, initial metal concentration, adsorbent dosage and solution pH were evaluated. Data obtained were subjected to adsorption isotherms, kinetic modeling and thermodynamic studies.

2. Materials and methods

Cadmium chloride ($CdCl_2{\cdot}2H_2O$), Zinc sulphate ($ZnSO_4{\cdot}7H_2O$), Sodium hydroxide (NaOH), Hydrochloride acid (HCl 35%) were AR grade supplied by Merck (India). Other reagents were of analytical grade and MilliQ water was used for reagent preparations.

2.1. Preparation of biosorbent powder from fish scale

Tilapia fish scales were collected from a local market in Karaikudi, Tamil Nadu, thoroughly washed with hot water to remove dirt and odour, then oven dried at 100°C overnight. The dried scales were then subjected to calcinations in a box furnace at temperature of 1000°C at heating rate of 5°C min^{-1}. The resulting solid was pulverized by grinding using mortar and pestle to obtain fine powder labelled Fish scale powder (FSP).

2.2. Characterization

X-ray diffraction (XRD) technique obtained with a PAN Analytical X'Pert PRO X-ray diffractometer with CuK α radiation (λ =1.5418 Å) was used for the crystal structure analysis. Fourier transform infrared (FT-IR) spectra were recorded from 400 to 4000 cm^{-1} in TENSOR 27 spectrometer (Bruker, Germany) using KBr pellets. The SEM images and EDAX were examined with S-4800 scanning electron microscopy (HITACHI, Japan). TEM micro graphs were taken with a JEOL-JEM-2010 (JEOL, Japan) operated at 200 kV. Thermogravimetric analysis and Differential thermal analysis were performed on SDT Q600 V8.3 Build 101 simultaneous DSC–TGA, equipped with Universal V4.7A TA software package while the particle size distribution was determined with Nanotrac equipped with Microtrac FLEX 10.5.2 software. The pH point of zero charge (pHpzc) for FSP was determined by contacting 0.1 g of each of the sample with 50 ml aqueous solution of 0.1 M NaCl whose initial pH had previously been adjusted between pH 2 and 10 with either NaOH or HCl. The mixtures were sealed and shake for 24 h, the final pH values were measured. The difference between the initial and final pH was calculated and plotted against the initial pH. The point of intersection of the resulting curve with vertical axis gave the pHpzc [19].

2.3. Preparation of aqueous solution of metal ions

The aqueous solutions of Cd^{2+} and Zn^{2+} (1000 mg L^{-1} each) were prepared from analytical grade of $CdCl_2{\cdot}2H_2O$ and $ZnSO_4{\cdot}7H_2O$ by dissolving 1.950 g and 4.398 g of the salts respectively in 1% HNO_3 solution prepared from distilled de-ionized water in 1000 ml flask. Working standard solutions were obtained from the stock solution by further dilution with de-ionized, the pH of the solutions were adjusted to desired values with aliquots of 1.0 mol L^{-1} of HCl and NaOH prior to the adsorption process.

2.4. Adsorption studies

The adsorption processes were conducted by contacting 100 ml of Cd^{2+} and Zn^{2+} (40, 80, 120, 160 and 180 mg L^{-1}) solutions with 0.16 g L^{-1} of FSP, agitated on orbital shaker at 30 ± 1°C at a speed of 100 rpm. The samples were collected at time intervals of 0, 5, 10, 15, 20, 30, 60 120 and 240 min and the adsorbent were separated by filtration. The adsorption isotherms were studied in the concentration range of 10–100 mg L^{-1} at pH 6 and contact time 72 h to reach equilibrium of the solid-solution mixture. The concentrations of the ions in the solutions before and after adsorption processes were estimated using UNICAM 929 Model Flame absorption spectroscopy equipped with hollow cathode lamp. The amounts of metal ion removed at time t, Q_t (mg g^{-1}) and at equilibrium Q_e (mg g^{-1}) were calculated using Eqs. (1) and (2) below:

$$Q_t = \frac{(C_o - C_t)V}{W} \quad (1)$$

$$Q_e = \frac{(C_o - C_e)V}{W} \quad (2)$$

where C_o (mg/L) is the initial concentration and C_t (mg L^{-1}) is the concentration of the metal ion at time t in the liquid-phase. C_e (mg L^{-1}) is the concentration of the metal ion

at equilibrium in the liquid-phase V is the volume of the solution (L), and W (g) is the mass of adsorbent.

3. Adsorption kinetic studies

The mechanism of the adsorption of Cd^{2+} and Zn^{2+} were investigated by subjecting kinetics data to pseudo-first order, pseudo-second-order, Elovich and Intra-particle diffusion model. The least square fit was used to obtain the parameters using Micro Math scientist software.

3.1. The pseudo-first order kinetics model

The pseudo-first order kinetics model assumed assumes that the rate of occupation of sorption sites is proportional to the number of unoccupied sites and can be represented by Eq. (3) below [19].

$$\frac{dQ}{dt} = k_1(Q_e - Q_t) \tag{3}$$

Upon integration with initial conditions of $Q_t = 0$ at $t = 0$, and $Q_t = Q_t$ at time, t and upon rearrangement, Eq. (3) transformed to Eq. (4) below

$$Q_t = Q_e(1 - e^{-k_1 t}) \tag{4}$$

where Q_e and Q_t are the solute concentrations (mg g^{-1}) at equilibrium and at time t (min), respectively, and k_1 the adsorption rate constant (min^{-1}), and t is the contact time (min). The values of Q_e and k_1 were calculated from the least square fit of Q_t vs. t at different metal ions concentrations.

3.2. The pseudo-second order kinetics model

Pseudo-second order kinetics model assumes that the rate of adsorption is limited chemical interactions involving valence forces through sharing or exchange of electrons between adsorbate and adsorbent. The model is as given by Eq. (5) below on assumption of equilibrium interactions between valence forces during adsorption process [20].

$$Q_t = \frac{k_2 Q_e^{\,2} t}{1 + k_2 Q_e t} \tag{5}$$

The values of Q_e and k_2 (g mg^{-1} min^{-1}), the rates constant of pseudo-second order adsorption process were calculated from the least square fit of Q_t vs. t at different solutes concentrations.

3.3. Elovich model

Elovich kinetic model is often used to describe the predominantly chemical sorption on highly heterogeneous sorbents however, it doesn't propose any definite mechanism for the interactions [21–23]. Elovich model is generally expressed as shown in Eq. (6)

$$Q_t = {}^{1}\!/\!_{\beta} \ln(\alpha\beta * t) \tag{6}$$

The constant α, the initial adsorption rate (mg g^{-1} min^{-1}) and β, the desorption constant (g mg^{-1}) are related to the rate of the chemisorption and surface coverage respectively with their interpretations usually connected to the heterogeneous surfaces [24,25].

3.4. Intra-particle diffusion model

The intra particle diffusion model [Eq. (7)] was applied to elucidate the diffusion mechanism during adsorption. Unlike all other kinetic models, this model describes adsorption mechanism controlled by diffusion within the pores rather than surface-related energy controls. The model proposed that the initial diffusion rate is dependent on contact time and surface resistance created by the concentration gradient across the surface.

$$Q_t = K_{id} t^{0.5} + C_i \tag{7}$$

where K_{id} is the intra particle diffusion rate constant (mg g^{-1} $min^{-0.5}$) and C_i is intercept and a measure of surface thickness [26].

4. Adsorption isotherms

Data from the equilibrium studies were analyzed with four common adsorption isotherm models namely, Langmuir, Freundlich, Dubinin–Radushkevich and Temkin isotherm. The isotherm parameters were obtained by the least square fit method.

4.1. Langmuir isotherms

The Langmuir isotherm equation is given by Eq. (3) based on assumptions that the entire surface for the adsorption has the same activity for adsorption and that there is no interaction between adsorbed molecules. Also, all the adsorptions were assumed to occur by the same mechanism and the extent of adsorption is less than one complete mono molecular layer on the surface [27].

$$Q_{eq} = \frac{Q_{\max} b C_e}{1 + b C_e} \tag{8}$$

where Q_{max} is the maximum amount of the solute adsorbed per unit weight of the adsorbent required to form a complete mono layer on the surface C_e (mg g^{-1}) is the concentration of the solute remaining in the solution at equilibrium and b is equilibrium constant (dm^3 mg^{-1}). The essential features of the Langmuir isotherm can be expressed in terms of a dimensionless constant separation factor, R_L which is related to b and initial concentration C_o by the expression; $R_L = 1/(1+bC_0)$. The value of R_L can be used to evaluate the nature of adsorption obtained from Langmuir isotherm, R_L of zero value indicates irreversible adsorption, the process is favourable when $0 < R_L < 1$, linear when $R_L = 1$ and unfavourable when $R_L > 1$.

4.2. Freundlich isotherm

The Freundlich isotherm is an empirical equation based on sorption on a heterogeneous surface, represented by Eq. (9):

$$Q_{eq} = K_F C_e^{1/n} \quad (9)$$

where K_F and n are the Freundlich constants related to the adsorption capacity and intensity of the sorbent, respectively [28].

4.3. Temkin isotherm model

In order to account for the interaction between sorbent and adsorbent, Temkin isotherm model [Eq. (10)] was applied to analyse the equilibrium data. The model proposed that the free energy of sorption is a function of the surface coverage [29].

$$Q_e = \frac{RT}{b_T} \ln a_T C_e \quad (10)$$

where, T is the temperature (K), and R is the ideal gas constant (8.314 J mol^{-1} K^{-1}) and 'a_T' and 'b_T' are constants relating to binding constant (L mg^{-1}) at equilibrium corresponding to the maximum binding energy and the heat of adsorption respectively.

4.4. The Dubinin–Radushkevich isotherm

The Dubinin–Radushkevich model [Eq. (11)] is more general than the Langmuir isotherm and can be used to estimate the heterogeneity of the surface energies as well as classification of adsorption processes into physiorption or chemisorption.

$$Q_e = Q_s e^{-\beta\varepsilon^2} \quad (11)$$

where Q_s is the theoretical saturation capacity (mol g^{-1}), ε is the Polanyi potential given by the relation; $\varepsilon = \ln(1 + 1/C_e)$, where C_e (mg L^{-1}), R (J mol^{-1} K^{-1}) and T (K) are as previously described. The constant β (mol^2 J^{-2}), is related to the mean free energy E (kJ mol^{-1}) of adsorption per molecule of the adsorbate by $E = (2\beta)^{-0.5}$. The magnitude of E between 8 and 16 kJ mol^{-1} indicates a chemisorption process, while $E < 8$ kJ mol^{-1} suggests a physorption process [30].

5. Statistical test

The acceptability and the best fit of a model are typically based on the square of the correlation coefficients, R^2 which is appropriate for linearized models. In this study, the least square fit was employed for data fit; therefore, error distribution comparison is desirable. Three error functions were used to validate the fit kinetic models, they are: the sum square error function (SSE), root mean square error (RMSE) and composite fractional error (HYBRD) [31].

$$SSE = \sum_{i=1}^{N} (Q_{(\exp)} - Q_{(cal)})^2 \quad (12)$$

$$RMSE = \sqrt{\frac{\sum_{i}^{N} (Q_{(\exp)} - Q_{(cal)})^2}{N}} \quad (13)$$

$$HYBRD = \frac{100}{N-P} \sum_{i}^{N} \frac{(Q_{(\exp)} - Q_{(cal)})}{Q_{(\exp)}} \quad (14)$$

where N represents the number of data points and P are the numbers of the parameters in the model. The higher is the value of R^2 and the lower the value of SSE, RMSE and HYBRD errors the more acceptable the model.

6. Results and discussion

6.1. Characterization

The XRD patterns of the biosorbent before and after adsorption are as presented in Fig. 1, two main characteristic peaks at 25.89 and 31.79° corresponding to (002) and (211) planes were observed. Other standard planes such as (202), (210), (213), (300), (310), (322), (004) and (410) were also observed in the powder, the spectra matched well with standard JCPDS file no. 090432 corresponding to hydroxyapatite powder [32]. Decrease in peaks intensities coupled with broadening of peaks were observed after the adsorption of metal ions. Similarly, the appearance of fewer peaks after contaminants adsorption was observed as a result of the transformation of well poly-crystalline structure into amorphous structure. The SEM images of the biosorbent before and after adsorption study are presented in Fig. 2a and 2b respectively. Before adsorption, the morphology revealed rod-like particles which became distorted as the particles agglomerated upon the adsorption of the metal ions. TEM (Fig. 2c) affirmed that the of rod-like shape of the biosorbent with dimension estimated to be 12–72 nm long and 6–10 nm in breath. The selected area electron diffraction (SAED) showed spotted and continuous rings suggesting a polycrystalline grains. The elemental compositions analysis (Fig. 2d) showed the presence of O, Na, Mg, and Si. Worth of nothing is the presence of Ca and P in ratio of 1.76 suggesting a non-stoichiometric hydroxyapatite residue [32]. The thermal analysis of the biosorbent is shown in Fig. 3a. The actual weight losses were observed in three regions, the loss of 1.9% at 67.77°C was due to the evaporation of weakly entrapped water molecules, the second weight loss of 4.07 % at 260.38°C is attributed to organic components loss while of 5.79% weight loss between 260 and 616°C is attributed to the decomposi-

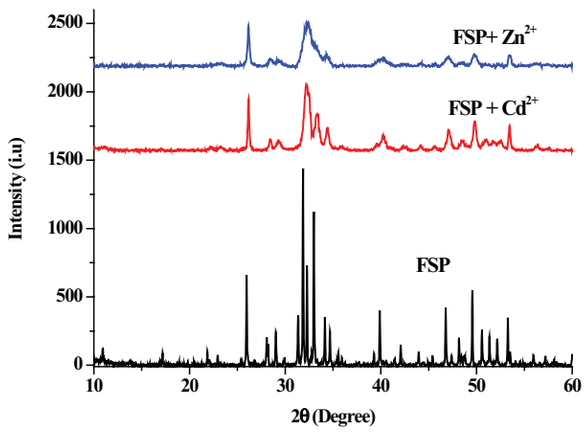

Fig. 1. XRD analysis of FSP before and after adsorption.

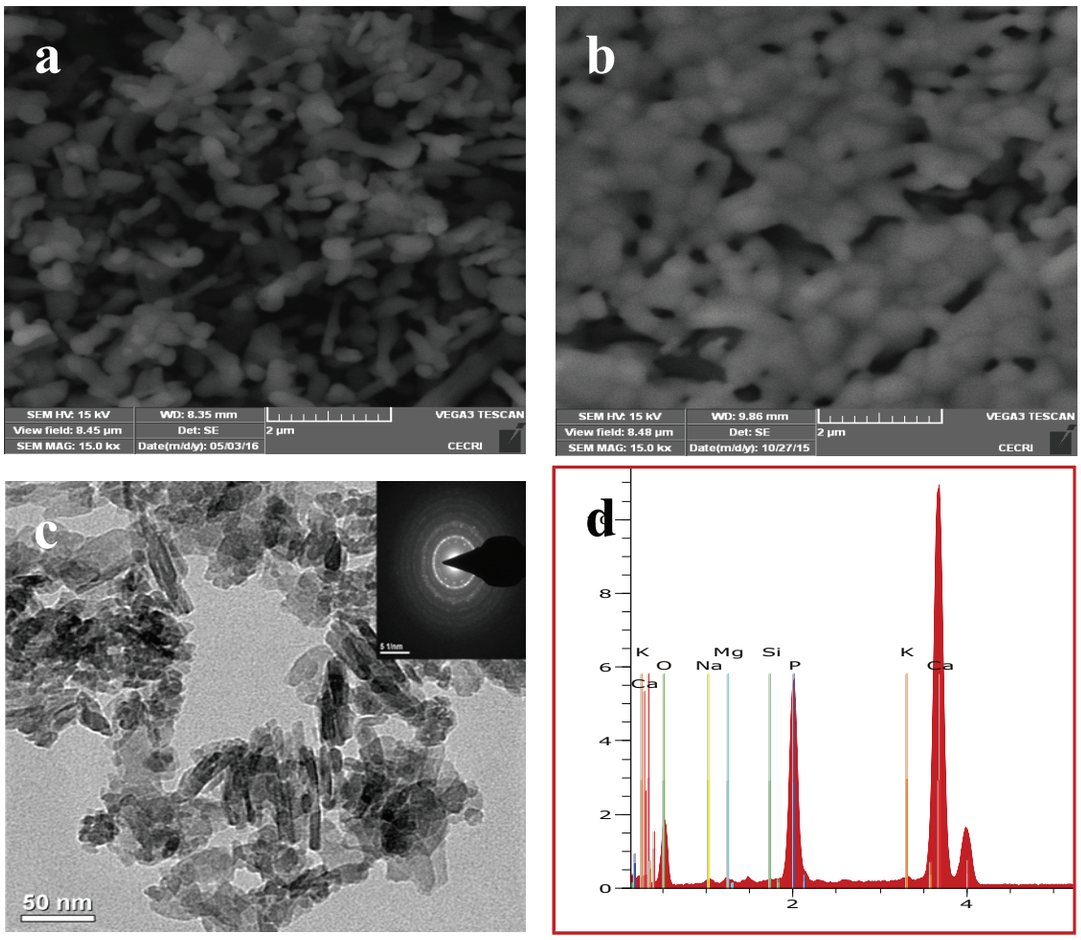

Fig. 2. SEM morphology of (a) before (b) after adsorption (c) TEM (d) EDAX of FSP.

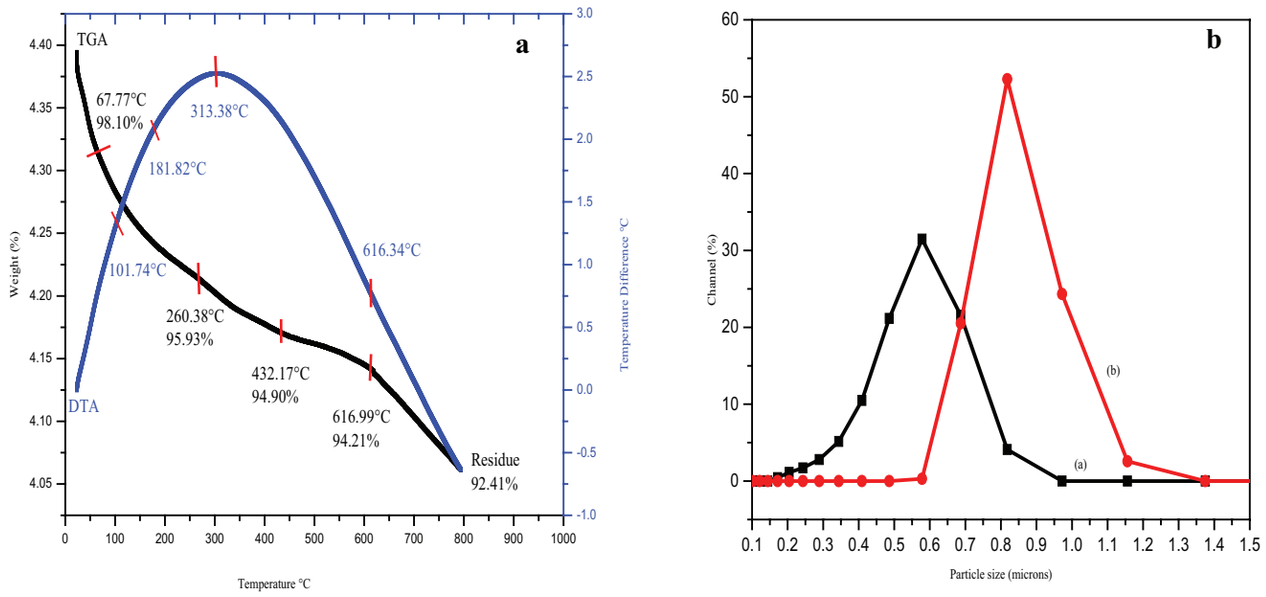

Fig. 3. TGA/DTA and particle size distribution of the FSP.

Table 1
Physical properties of the biosorbent prepared from Fish scale

Parameters	FHAp
Surface area (m^2/g)	83.11
Average pore size (nm)	1.55
Pore volume (cm^2/g)	0.26
Bulky density (g/cm^2)	2.73
Ash content (%)	2.61
pHZPC	6.32

tion of the scales. The weight loss between 400 and 600°C and even beyond indicates thermal stability of the biosorbent in this range. A total weight loss of 7.59% was noticed, while a residue of 92.41% was achieved. DTA analysis shows a sharp exothermic peak in the range from 400–800°C, which is an indication of crystallization of hydroxyapatite powder. The average particle size distribution of the raw and calcined fish scales are presented in Fig. 3b, before calcination, the particle distribution was 850 nm which reduced to 550 nm after sintering indicating a reduction in particle size. The physical properties of the biosorbent are presented in Table 1.

The FT-IR spectra of biosorbent prepared from fish scale before and after adsorption are shown in Fig. 4. The appearance of a strong and most intensive broad band centered at about 1026–1048 cm^{-1} due to asymmetric stretching mode vibration of PO_4 group [33,34]. The vibration bands of O–P–O bending molecules (υ_4) were observed to range from 560 to 604 cm^{-1}. The bands found between 864 and 1450 cm^{-1} are assigned to the stretching vibrations of CO_3^{2-} which is in line with carbonate ion reported around 864 and 1434 cm^{-1} [35]. The bands with the highest wave number range from 3436 to 3633 cm^{-1} indicate the vibration of O–H bonds which show similarity with 3435 cm^{-1} and 3600 cm^{-1} [36]. The presence of peak in the region of 1640 cm^{-1} was due to absorbed water molecule. The appearance of broadening and shift in peak positions were prominent after the adsorption could be ascribed to incorporation of adsorbed ions into the biosorbent structure.

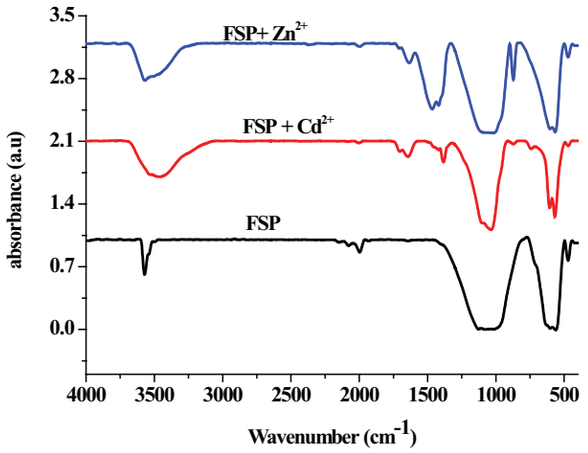

Fig. 4. FTIR Spectra of the biosorbent (FSP) before and after adsorption.

7. Adsorption study

7.1. Effects of contact time and initial concentrations of metalions

The effects of contact time and initial metals concentration on the biosorption process are as shown in Fig. 6. The process is characterized by a rapid biosorption in the first thirty minutes followed by a moderate progress in the next ninety minutes after which the processes finally display quasi-equilibrium. These observations may be attributed to gradual occupation of the vacant sites and functional group available for the metal ions. The adsorption capacity of the biosorbent increases from 22.1 to 122.7 mg g^{-1} for Cd^{2+} and 20.5 to 113.6 mg g^{-1} for Zn^{2+} as the initial concentration increases from 40 to 240 mg L^{-1}.

8. Effects of solution pH and adsorbent dosage

The pH of the medium is one of the determining factors in biosorption process because pH changes affect the chemistry of both adsorbate and adsorbent. The effect of pH on the biosorption of Cd^{2+} and Zn^{2+} are as presented in Fig. 6a. At lower solution pH, there are more H^+ in the solution, the competition for the available adsorption sites by the H^+ and the metal ions is likely responsible for lower efficiency recorded at low pH. Increase pH led to exposure of more adsorption sites, the maximum adsorption capacities of about 88% and 82% for Cd^{2+} and Zn^{2+} were obtained around pH of 6.5. Adsorption capacities decreases with further increase in pH, this may be attributed to the formation of metal hydroxides and their eventual precipitation [37].

The effect of adsorbent dose on percentage metal ions removed is as shown in Fig. 6b. The increased is due to the availability of adsorption sites on the surface of the adsorbent which enhances the uptake of the pollutants from aqueous solution. However, the capacity decreased with the increasing amount of adsorbent when expressed in mg per g^{-1} of the adsorbent. This is due to aggregation of adsorption sites resulting in a decrease in total adsorbent surface area available to the metal ions and an increase in diffusion path length.

9. Adsorption kinetics study

The biosorption mechanism and efficiency of the biosorbent were investigated through the kinetic of the biosorption process. The kinetics of biosorption Cd^{2+} and Zn^{2+} by FSP were investigated using four common kinetic models earlier presented. The least square fits of the experimental data with the model are presented in Figs. 7a–d and 8a–d, while the parameters for the fits are shown in Tables 2 and 3. It is obvious from Tables 2 and 3 that the biosorption process followed the pseudo-first-order with strong correlation coefficient (R^2) and it was probably dominated by a physical adsorption phenomenon [38]. In addition, the values of Q_e obtained from the model are consistent with the experimental values ($Q_{e\,exp}$), also the statistical errors are lower when compared with that of second order parameters.

Tables 2 and 3 as well as Figs. 7c and 8c show that the Elovich kinetic plot fitted well with highly significant correlation coefficients (R^2) value for both for Cd^{2+} and Zn^{2+}. The

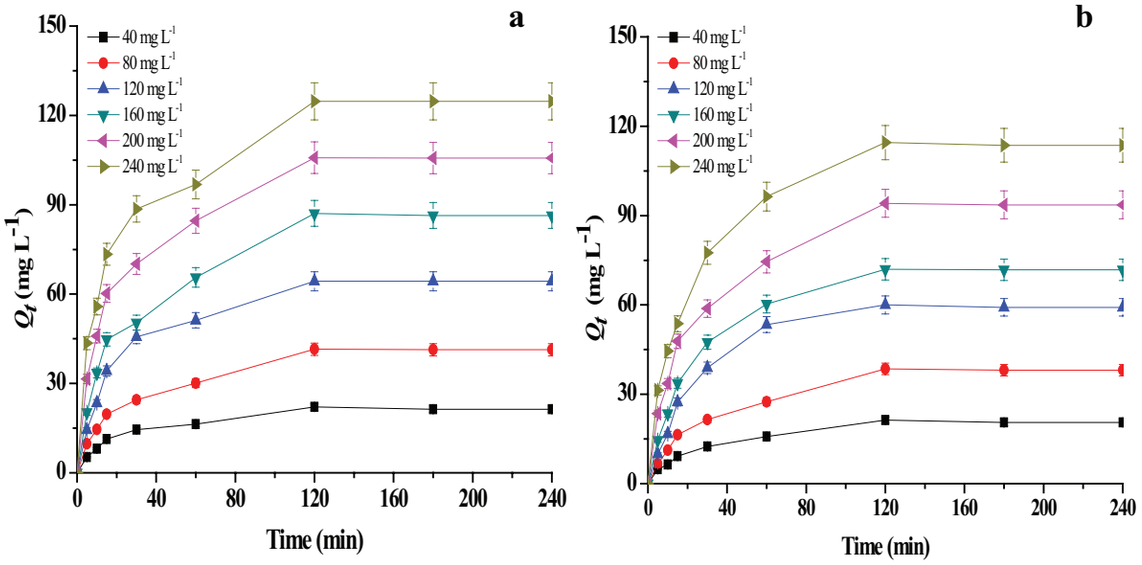

Fig. 5. Effects of contact time and initial concentrations on biosorption of (a) Cd^{2+} (b) Zn^{2+}. (Condition: pH = 7; adsorbent dosage of 0.16 gL^{-1}; temperature 30°C).

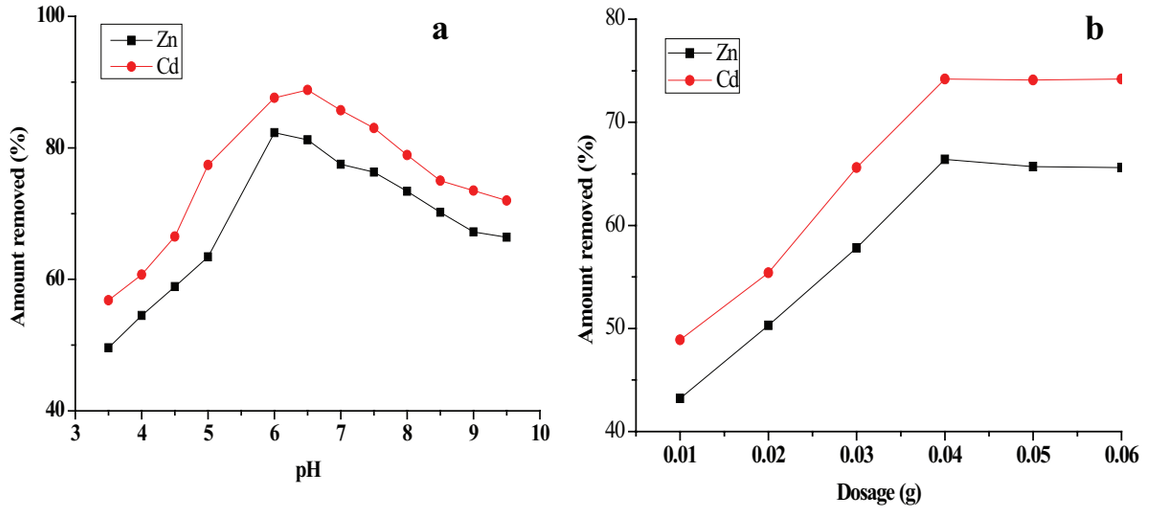

Fig. 6. The effect of (a) solution pH (b) biosorbent dosage on metal ions removal efficiency.

initial adsorption rate constant, α for Cd^{2+} and Zn^{2+} range from 2.67 to 38.86 and 2.42 to 18.49 mg (g min)$^{-1}$ respectively as their initial concentrations increase from 40 to 240 mg L^{-1}. This shows that biosorption of Cd^{2+} onto FSP is higher than that of Zn^{2+}, this may be attributed to higher electro negativity and lower enthalpy of hydration of Cd^{2+} compared with Zn^{2+}. Interestingly, both metal ions display similar range of desorption constant, β which decrease as the concentration increases indicating a physiochemical interaction between the ions and the functional groups present on the FSP.

The biosorption mechanism was investigated using intra particle diffusion model. Figs. 7d and 8d show that the uptake of the metal ions is a function of $t^{0.5}$ with two distinct diffusion portions. These portions may be attributed to the rapid intra particle diffusion of the metal ions into the interior pores of the biosorbent particle and the final equilibrium state as a result of slow intra particle diffusion as the metal ion concentrations in the solution decrease [39]. Tables 2 and 3 show that the plots for Cd^{2+} and Zn^{2+} do not pass through the origin and exhibited multilinearity, which indicated the presence of two steps mentioned above [40]. The first step has the biggest K_{id} values and exhibits higher speed than the other step due to the availability of vacant sites.

The isotherms study is meant for biosorbent performance assessment which provides information on the feasibility of removing metal ions, surface properties and affinity of the biosorbent for the biosorbate [41]. The least fits of equilibrium data with the isotherm models are pre-

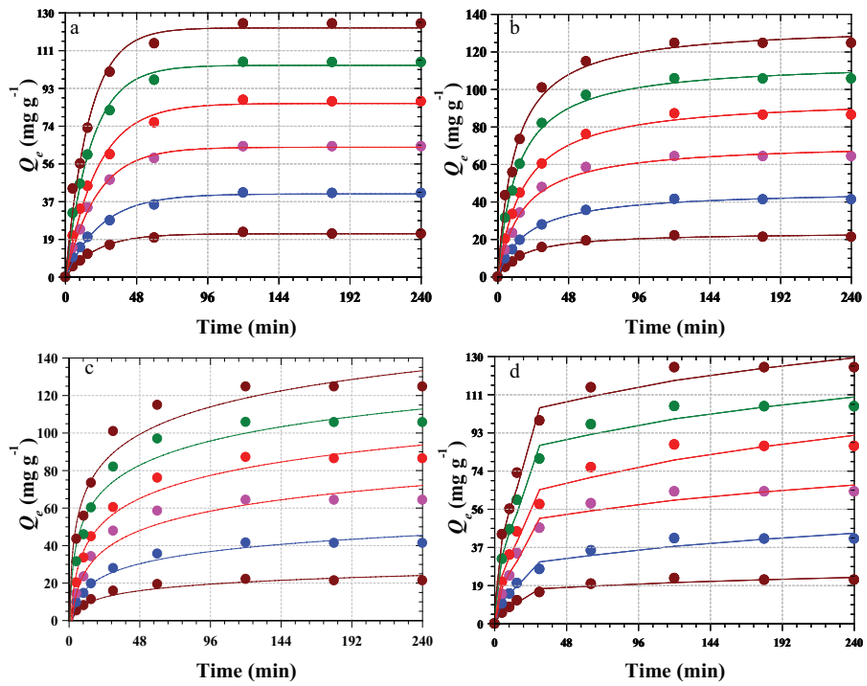

Fig. 7. Kinetic fits for the biosorption of Cd^{2+} (a) pseudo-first order model fits (b) pseudo-second order model fits (c) Elovich and (d) Intra particle diffusion model fits.

Table 2
Kinetic parameters for the adsorption of Cd^{2+} on to FSP

	C_o (mg/L)	40.00	80.00	120.00	160.00	200.00	240.00
Pseudo-first order	$Q_{e\,exp}$ (mg g^{-1})	22.10	41.50	64.30	87.10	105.80	124.70
	$Q_{e\,cal}$ (mg g^{-1})	21.46	41.20	64.15	86.06	104.85	123.48
	$k_1 \times 10^2$ (min^{-1})	4.69	4.04	4.68	4.50	5.62	6.18
	R^2	0.999	0.998	0.999	0.999	0.999	0.998
	%SSE	0.084	0.005	0.001	0.014	0.008	0.010
	RMSE	0.080	0.038	0.019	0.130	0.119	0.153
	HYBRD	0.362	0.092	0.029	0.150	0.113	0.123
Pseudo-second order	$Q_{e\,cal}$ (mg g^{-1})	23.10	45.27	70.14	93.66	112.04	130.62
	$k_2 \times 10^4$ (g mg^{-1} min^{-1})	25.3	10.4	8.17	5.56	6.25	6.25
	R^2	0.997	0.999	0.998	0.999	0.999	0.998
	%SSE	0.207	0.826	0.825	0.567	0.348	0.226
	RMSE	0.126	0.471	0.730	0.820	0.780	0.741
	HYBRD	0.568	1.136	1.135	0.941	0.737	0.594
Elovich	$Q_{e\,cal}$ (mg g^{-1})	19.79	37.42	59.99	78.50	97.46	115.71
	α (mg (g min)$^{-1}$)	2.67	5.24	8.94	12.75	25.21	38.86
	β (g mg^{-1})	0.214	0.114	0.073	0.057	0.052	0.046
	R^2	0.998	0.999	0.998	0.999	0.999	0.998
	%SSE	0.011	0.010	0.004	0.010	0.006	0.005
	RMSE	0.289	0.511	0.539	1.075	1.043	1.123
	HYBRD	1.306	1.230	0.838	1.234	0.986	0.901
Intra-particle diffusion	K_{1d} (mg g^{-1} min$^{-0.5}$)	2.40	4.34	7.42	9.14	11.65	13.87
	C_1 (mg g^{-1})	0.53	0.71	0.84	2.40	6.01	9.52
	R^2	0.991	0.941	0.957	0.984	0.988	0.983
	K_{2d} (mg g^{-1} min$^{-0.5}$)	0.75	1.79	2.01	3.69	3.67	4.00
	C_2 (mg g^{-1})	11.17	16.77	36.55	35.99	55.41	69.41
	R^2	0.994	0.994	0.997	0.993	0.996	0.996

Table 3
Kinetic parameters for the adsorption of Zn^{2+} on to FSP

	C_o (mg/L)	40	80	120	160	200	240
Pseudo-first order	$Q_{e\,exp}$ (mg g^{-1})	20.50	38.10	59.20	71.80	93.60	113.60
	$Q_{e\,cal}$ (mg g^{-1})	20.33	37.75	59.40	71.32	91.94	112.14
	$k_1 \times 10^2$ (min^{-1})	3.66	3.22	3.69	3.97	4.26	4.51
	R^2	0.998	0.999	0.998	0.997	0.999	0.998
	%SSE	0.007	0.009	0.001	0.005	0.032	0.017
	RMSE	0.021	0.044	0.025	0.060	0.208	0.183
	HYBRD	0.104	0.116	0.041	0.084	0.222	0.161
Pseudo-second order	$Q_{e\,cal}$ (mg g^{-1})	22.98	43.41	67.63	81.99	102.97	124.47
	$k2 \times 10^4$ (g mg^{-1} min^{-1})	19.7	8.76	6.49	5.54	5.25	4.73
	R^2	0.998	0.999	0.997	0.998	0.998	0.998
	%SSE	1.463	1.945	2.029	2.014	1.001	0.916
	RMSE	0.310	0.664	1.054	1.274	1.171	1.359
	HYBRD	1.512	1.743	1.781	1.774	1.251	1.196
Elovich	$Q_{e\,cal}$ (mg g^{-1})	18.95	34.72	55.63	67.23	87.16	106.75
	α (mg (g $min)^{-1}$)	2.42	3.70	6.28	8.77	13.67	18.49
	β (g mg^{-1})	0.219	0.113	0.072	0.062	0.051	0.043
	R^2	0.995	0.996	0.992	0.994	0.995	0.994
	%SSE	0.0057	0.0079	0.0036	0.0041	0.0047	0.0036
	RMSE	0.194	0.423	0.447	0.572	0.805	0.856
	HYBRD	0.945	1.110	0.755	0.796	0.860	0.754
Intra-particle diffusion	K_1d (mg g^{-1} $min^{-0.5}$)	2.32	4.16	7.24	8.60	10.83	13.52
	C_1 (mg g^{-1})	-0.26	-1.05	-2.80	-1.68	0.60	1.13
	R^2	0.999	0.997	0.992	0.997	0.998	0.999
	K_2d (mg g^{-1} $min^{-0.5}$)	0.83	1.75	1.83	2.38	3.52	3.54
	C_2 (mg g^{-1})	9.34	14.20	34.74	39.41	45.51	65.49
	R^2	0.994	0.994	0.997	0.993	0.996	0.996

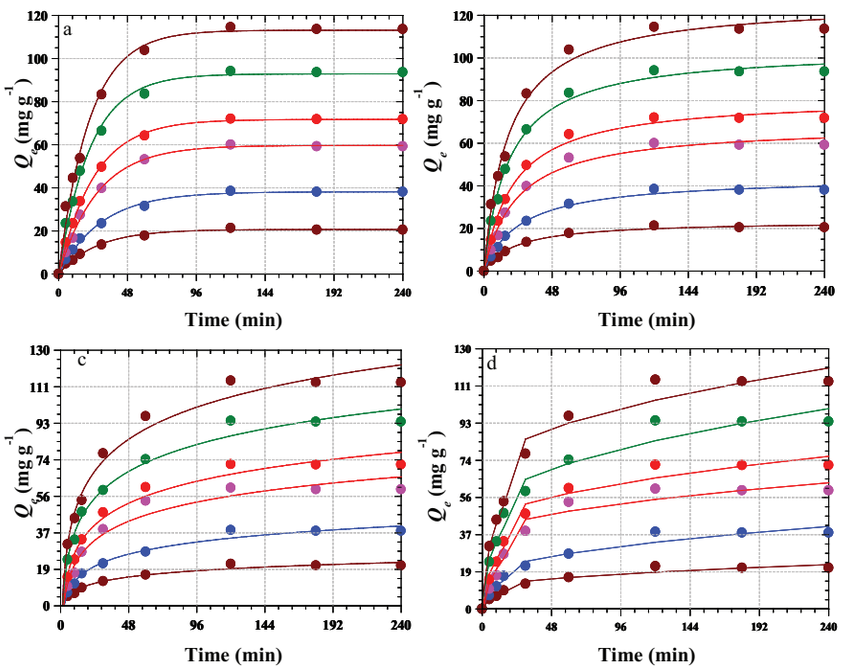

Fig. 8. Kinetic fits for the adsorption of Zn^{2+} (a) pseudo-first order model fits (b) pseudo-second order model fits (c) Elovich and (d) Intra particle diffusion model fits.

sented in Figs. 9a,b while the fitting parameters are presented in Table 4. Maximum adsorption capacities (Q_{max}) of 112.57 and 95.69 mg g^{-1} were obtained for the Langmuir mono layer adsorption with separation factor, R_L of 0.12 and 0.17 while the Freundlich isotherm parameters, n were 2.92 and 2.79 respectively for Cd^{2+} and Zn^{2+}. These indicate a favourable biosorption process. Theoretical saturation capacityies (Q_s), of 91.89 and 75.78 mg g^{-1} were obtained respectively for Cd^{2+} and Zn^{2+} from Dubinin–Radushkevich model which is less than the maximum adsorption capacities of the metal ions. The maximum adsorption energies, E, of 0.19 and 0.14 kJ mol^{-1} obtained respectively for Cd^{2+} and Zn^{2+} show that their biosorption onto FSP is physisorption dominated process. When compared, the values of correlation coefficient (R^2) show that the models fit the isotherm in the order of Dubinin–Radushkevich > Langmuir > Temkin > Freundlich for Cd^{2+} and Langmuir > Temkin > Dubinin–Radushkevich > Freundlich for the Zn^{2+} with the R^2 values are greater than 0.9 in all the models. The results obtained in this study compared favourably well with other sorbents reported in literature (Table 5).

10. Thermodynamic study

The distribution of the metal ion between the solution and the biosorbent at equilibrium is written as: where K_D is the equilibrium constant

$$K_D = \frac{M^{n+}{}_{biosoebed}}{M^{n+}_{solution}} = \frac{Q_e}{C_e}$$

The equilibrium constant K_D is a function of temperature, thus can be used is used in the determination the thermodynamics parameters. The thermodynamics parameters i.e. $\Delta G°$, $\Delta H°$ and $\Delta S°$ were estimated using the vant Hoff equation [47] as follow:

$$\Delta G^o = -RT \ln K_D \quad (15)$$

$$\ln K_D = \frac{\Delta H^o}{RT} - \frac{\Delta S}{R} \quad (16)$$

A plot of $ln\ K_D$ vs $1/T$ gives a straight line graph (Fig. 10) with slope as $\frac{\Delta H^o}{R}$ and intercept as $\frac{\Delta S}{R}$. The thermodynamics parameters are shown in Table 5.

The values of $\Delta G°$ are negative which implies that biosorption is thermodynamically feasible and spontaneous in nature. The decrease values $\Delta G°$ as the temperature increases implies that the process becomes more feasible as temperature increases. The positive values of $\Delta H°$ obtained for the two metal ions indicated endothermic nature of the biosorption processes. The positive $\Delta S°$ values implied increase randomness at the solid/

Table 4
Isotherm parameters for the biosorption of Cd^{2+} and Zn^{2+} on to FSP

Isotherms	Parameter	Cd^{2+}	Zn^{2+}
Langmuir	Q_{max} (mg g^{-1})	112.57	95.69
	b (L mg^{-1})	0.07	0.05
	R_L	0.12	0.17
	R^2	0.973	0.992
Freundlich	$K_F \times 10^2$ ((mol g^{-1}) (mol L^{-1})$^{-1/n}$	21.65	15.38
	n	2.92	2.79
	R^2	0.959	0.980
Temkin	a_T (L mg^{-1})	98.80	116.88
	b_T	0.59	0.42
	R^2	0.970	0.989
Dubinin–Radushkevich	Q_s (mg g^{-1})	91.89	75.78
	$\beta \times 10^6$ (mol J^{-1})^2	1.35	2.70
	E (kJ mol^{-1})	0.19	0.14
	R^2	0.978	0.982

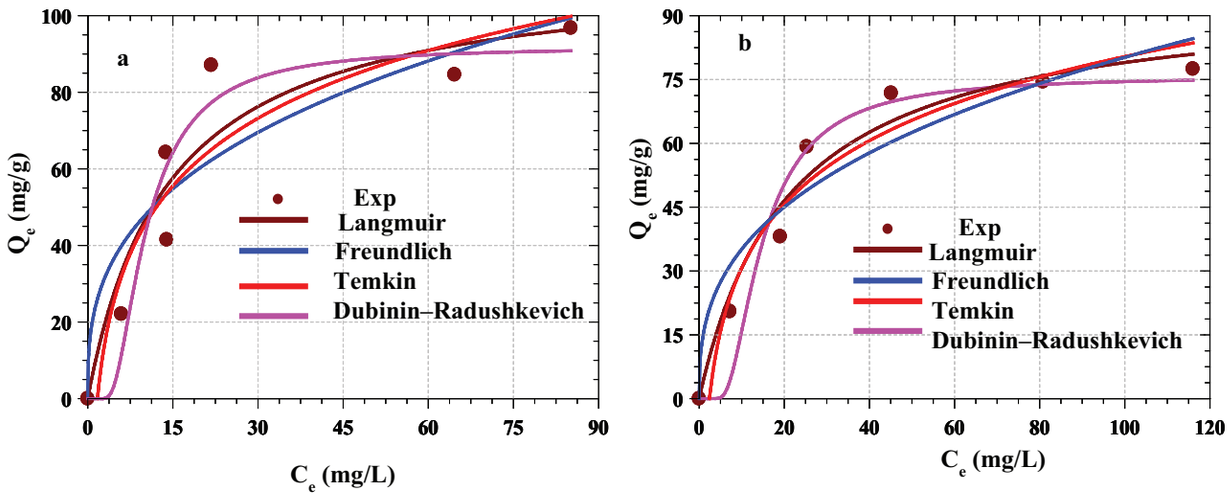

Fig. 9. Isotherm fits for the adsorption of (a) Cd^{2+} (b) Zn^{2+} onto FSP.

Table 5
Comparison of sorbents for biosorption of Cd^{2+} and Zn^{2+}

Adsorbent	Adsorption capacity (mg g^{-1})		Ref
	Cd^{2+}	Zn^{2+}	
Bentonite	7.40	1.31	[42]
Functionalized silica nanoparticles	199.00	133.00	[43]
Magnetic hydroxyapatite nanoparticles	220.78	140.65	[44]
L. hyperborea	31.30	19.20	[45]
S. muticum	38.40	34.10	[45]
F. spiralis	42.10	34.30	[45]
B. bifurcata	30.30	30.30	[45]
Padina sp.	84.31	52.97	[46]
Sargassum sp.	85.43	32.70	[46]
Ulva sp.	65.20	35.31	[46]
Gracillaria sp.	33.72	26.16	[46]
Calcinated fish scale	112.57	95.69	This study

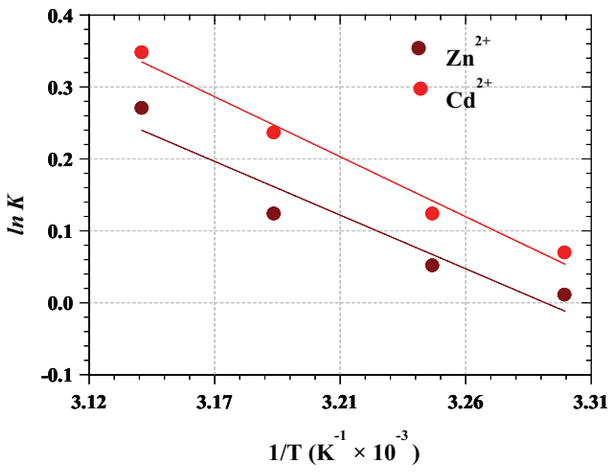

Fig. 10. Thermodynamic fits for the adsorption of Cd^{2+} and Zn^{2+} onto FSP.

solution interface during the biosorption process for the metal ions.

11. Conclusion

This study revealed the feasibility of preparation of biosorbent from Tilapia fish scale via calcination for the removal of Cd^{2+} and Zn^{2+} from aqueous solution in batch processes. The characterization of biosorbent using XRD, EDAX, SEM and FTIR showed that the prepared biomass has crystalline structure with well resolved functional groups. Biosorption process depends on initial metal ion concentrations, contact time, biosorbent dosage, temperature and pH. The pseudo-first-order kinetic model was found to be the most suitable to forecast the adsorption behaviour of the adsorbent and intra-particle diffusion was not the sole rate controlling factor. Equilibrium data fitted very well in the Langmuir isotherm equation, confirming the mono layer adsorption capacities of Cd^{2+} and Zn^{2+} with a mono layer adsorption capacity of 112.57 and 95.69 mg g^{-1} respectively at 301 K. The thermodynamics parameters indicate a favourable endothermic biosorption process. These findings suggest that calcined Tilapia fish scale is an inexpensive and effective biosorbent for Cd^{2+} and Zn^{2} removals from aqueous solutions.

Acknowledgements

One of the authors (Ofudje E.A) is grateful to the Government of India, Department of Science and Technology (DST) for RTF-DCS Fellowship Award and also to the authority of McPherson University, Ogun State, Nigeria, for granting the study leave to execute the fellowship. All authors wish to appreciate the technical staff of Central Instrumentation Facility (CIF) and Dr. Deepak K. Pattananyak of CSIR-CECRI for their numerous supports.

References

[1] A.A. Alqadami, Mu. Naushad, Z.A. ALOthman, A.A. Ghfar, Novel metal–organic framework (MOF) based composite material for the sequestration of U (VI) and Th (IV) metal ions from aqueous environment, ACS Appl. Mat. Interfaces, 9 (2017) 36026–36037.
[2] P. Trivedi, L. Axe, Modelling Cd and Zn sorption to hydrous metal oxides, Environ. Sci. Technol., 34 (2000) 2215–2223.

Table 5
Thermodynamic parameters for the adsorption of Cd^{2+} and Zn^{2+} on to FSP

	Cd^{2+}					Zn^{2+}				
Temp (K)	In K	ΔG° (J mol^{-1})	ΔH° (kJ mol^{-1})	ΔS° (J mol^{-1} K^{-1})	R^2	In K	ΔG° (J mol^{-1})	ΔH° (kJ mol^{-1})	ΔS° (J mol^{-1} K^{-1})	R^2
303	0.011	–26.98				0.069	–174.75			
308	0.052	–131.88	13.06	43.00	0.966	0.123	–316.23	14.61	48.64	0.996
313	0.123	–321.36				0.236	–614.91			
318	0.270	–714.89				0.348	–919.28			

[3] D. Mohan, K.P. Singh, Single and multi-component adsorption of cadmium and zinc using activated carbon derived from bagasse-an agricultural waste, Water Res., 36 (2002) 2304–2318.
[4] B.C. Janegitz, L.C.S Figueiredo-Filho, L.H. Marcolino-Junior, S.P.N. Souza, E.R. Pereira-Filho, O. Fatibello-Filho, Development of a carbon nanotubes paste electrode modified with cross linked chitosan for cadmium (II) and mercury (II) determination, J. Electroanal. Chem., 660 (2011) 209–216.
[5] M. Iqbal, A. Saeed, S.I. Zafar, Hybrid biosorbent: An innovative matrix to enhance the biosorption of Cd (II) from aqueous solution, J. Hazard. Mater., 148 (2007) 47–55.
[6] M. Fleischer, A.F. Sarofim , D.W. Fassett, P. Hammond , H.T. Shacklette, I.C. Nisbet, S. Epstein , Environmental impact of cadmium: a review by the panel on hazardous trace substances, Environ. Health Perspect., 7 (1974) 253.
[7] M.R. Lewis, L. Kokan, Zinc gluconate: acute ingestion, J. Toxicol. Clin. Toxicl., 36 (1998) 99–101.
[8] S.P. Nations, P.J. Boyer, L.A. Love, M. Burritt, J.A. FButz, G.I. Wolfe, L.S. Hynan, J. Reisch, J.R. Trivedi, Denture cream: An unusual source of excess zinc, leading to hypocupremia and neurologic disease, Neurology, 71 (2008) 639–643.
[9] P.L. Hooper, L. Visconti, P.J. Garry, G.E. Johnson, Zinc lowers high-density liprotein-cholesterol levels, J. Am. Med. Assoc. 244 (1980)1960–1961.
[10] A. Mittal, M. Naushad, G. Sharma, Z.A. ALothman, S.M. Wabaidur, M. Alam, Fabrication of MWCNTs/ThO2 nano composite and its adsorption behavior for the removal of Pb (II) metal from aqueous medium, Desal. Water Treat., 57 (46) (2016) 21863–21869.
[11] G. Sharma, M. Naushad, D. Pathania, A. Mittal, G.E. El-Desoky, Modification of Hibiscus cannabinus fiber by graft copolymerization: Application for dye removal, Desal. Water Treat., 54 (11) (2015) 3114–3121.
[12] Volesky, Detoxification of metal-bearing effluents: biosorption for the next century, Hydrometallurgy, 59 (2001) 203–216.
[13] A. Pugazhendhi, G.M. Boovaragamoorthy, K. Ranganathan, Mu.Naushad, T. Kaliannan, New insight into effective biosorption of lead from aqueous solution using *Ralstonia solanacearum*: Characterization and mechanism studies, J. Cleaner Production, 174 (2018) 1234–1239.
[14] H.E.A. Tudor, C.C. Gryte, C.C. Harris,. Seashells: detoxifying agents for metal-contaminated waters, Water Air Soil Pollut., 173 (2006) 209–242.
[15] C. Gok, D.A. Turkozu, S. Aytas, Removal of Th(IV) ions from aqueous solution using bi-functionalized algae-yeast biosorbent, J. Radioanal. Nucl. Chem., 287(2) (2011) 533–541.
[16] A. Witek-Krowiak, R.G. Szafran, S. Modelski, Biosorption of heavy metals from aqueous solutions onto peanut shell as a low-cost biosorbent, Desalination, 265(1–3) (2011) 126–134.
[17] A.A. Kadir, A. Puade, The utilisation of activated carbon (AC) from palm shell waste to treat textile wastewater, Adv. Environ. Biol., 7(12) (2013) 3621–3627.
[18] M.O. Nkiko, A.I. Adeogun, N.A. Babarinde, O.J. Sharaibi, Isothermal, kinetics and thermodynamics studies of the biosorption of Pb (II) ion from aqueous solution using the scale of croaker fish (Genyonemuslineatus), J. Water Reuse Desal., 3(3) (2013) 239–248.
[19] M.C. Somasekhara Reddy, L. Sivaramakrishnab, A. Varada Reddy, The use of an agricultural waste material, jujuba seeds, for the removal of anionic dye (Congo red) from aqueous medium, J. Hazard. Mater., 203–204 (2012) 118–127.
[20] Y.S. Ho, D.A.J. Waste, C.F. Forster, Batch nickel removal from aqueous solution by sphagnum moss peat, Wat. Res., 29 (1995) 1327–1332.
[21] S.H. Chien, W.R. Clayton, Application of Elovich equation to the kinetics of phosphate release and sorption in soils, Soil Sci. Soc. Am. J., 44 (1980) 265–268.
[22] T. Mu. Naushad, A. Basheer, M. Al-Maswari, A.A. Alqadami, SM. Alshehri, Nickel ferrite bearing nitrogen-doped mesoporous carbon as efficient adsorbent for the removal of highly toxic metal ion from aqueous medium, Chem. Eng. J., 330 (2017) 1351–1360.
[23] A.A. Alqadami, Mu. Naushad, M.A. Abdalla, T. Ahmad, Z.A. ALOthman, S.M. ALShehri, A.A. Ghfar, Efficient removal of toxic metal ions from wastewater using a recyclable nano composite: A study of adsorption parameters and interaction mechanism, J. Cleaner Production, 156 (2017) 426–436.
[24] C. Aharoni, F.C. Tompkins, Kinetics of adsorption and desorption and the Elovich equation, Adv. Catal., 21 (1970) 1–49.
[25] G. Sharma, B. Thakur, Mu. Naushad, A.H. Al-Muhtaseb, A. Kumar, M. Sillanpaa, G.T. Mola, Fabrication and characterization of sodium dodecyl sulphate@ironsilico phosphate nano composite: Ion exchange properties and selectivity for binary metal ions, Mater. Chem. Phys., 193 (2017) 129–139.
[26] Z.A. ALOthman, M.M. Alam, Mu. Naushad, Heavy toxic metal ion exchange kinetics: Validation of ion exchange process of composite cation exchanger nylon 6,6 Zr(IV) phosphate, J. Ind. Eng. Chem., 19 (2013) 956–960.
[27] I. Langmuir, The constitution and fundamental properties of solids and liquids. Part I. Solids, J. Am. Chem. Soc., 38(11) (1916) 2221–2295.
[28] H. Freundlich, The uptake of substances on solid surfaces, Phys. Chem Soc., 40 (1906) 1361–1368.
[29] M.I. Temkin, V. Pyzhev, Kinetics of ammonia synthesis on promoted iron catalysts, Acta physio chim. URSS, 12(3) (1940) 217–222.
[30] M.M. Dubinin, L.V. Radushkevich, Equation of the characteristic curve of activated charcoal, Chem. Zentr, 1(1) (1947) 875.
[31] N. Narayanan, S. Gupta, V.T. Gajbhiye, K.M. Manjaiah, Optimization of isotherm models for pesticide sorption on biopolymer-nanoclay composite by error analysis, Chemosphere, 173 (2017) 502–511.
[32] A.I. Adeogun, A.E. Ofudje, M.A. Idowu, S.O. Kareem, Facile development of nano size calcium hydroxyapatite based ceramic from eggshells: synthesis and characterization, Waste Biomass Valorization, (2017) 1–5.
[33] H.K. Varma, S.S. Babu, Synthesis of calcium phosphate bioceramics by citrate gel pyrolysis method, Ceramics Inter., 31(1) (2005) 109–114.
[34] S. Bose, S. Dasgupta, S. Tarafder, A. Bandyopadhyay, Microwave-processed nano crystalline hydroxyapatite: Simultaneous enhancement of mechanical and biological properties, Acta biomaterialia., 6(9) (2010) 3782–3790.
[35] S. Sasikumar, R. Vijayaraghavan, Synthesis and characterization of bioceramic calcium phosphates by rapid combustion synthesis, J. Mat Sci Tech., 26(12) (2010) 1114–1118.
[36] T.R. Tatarchuk, N.D. Paliychuk, M. Bououdina, B. Al-Najar, M. Pacia, W. Macyk, A. Shyichuk, Effect of cobalt substitution on structural, elastic, magnetic and optical properties of zinc ferrite nano particles, J. Alloys Comp., 731 (2018) 1256–1266.
[37] X. Chen, J.V. Wright, J.L. Conca, L.M. Peurrung, Effects of pH on heavy metal sorption on mineral apatite, Environ. Sci. Technol., 31 (1997) 624–631.
[38] Y. Lin, H. Chen, K. Lin, B. Chen, C. Chiou, Application of magnetic particles modified with amino groups to adsorb copper ions in aqueous solution, J. Environ Sci., 23(1) (2011) 44–50.
[39] Mu. Naushad, Z.A. ALOthman, M. Islam Adsorption of cadmium ion using a new composite cation-exchanger polyaniline Sn(IV) silicate: Kinetics, thermodynamic and isotherm studies, Int. J. Env. Scie. Technol., 10 (2013) 567–578.
[40] Mu. Naushad, Z.A. ALOthman, M. Islam Adsorption of cadmium ion using a new composite cation-exchanger polyaniline Sn(IV) silicate: Kinetics, thermodynamic and isotherm studies, Int. J. Env. Sci. Technol., 10 (2013) 567–578.
[41] F. Googerdchian, A. Moheb, R. Emadi, Lead sorption properties of nanohydroxyapatite–alginate composite adsorbents, Chem. Eng. J., 200 (2012) 471–479.
[42] G. Bereket, A.Z. Arog, M.Z. Özel, Removal of Pb (II), Cd (II), Cu (II), and Zn (II) from aqueous solutions by adsorption on bentonite, J. Colloid Interface Sci., 187(2) (1997) 338–343.

[43] X.F. Kong, B. Yang, H. Xiong, Y. Zhou, S.G. Xue, B.Q. Xu, S.X. Wang, Selective removal of heavy metal ions from aqueous solutions with surface functionalized silica nano particles by different functional groups, J. Cent. South Univ., 21(9) (2014) 3575–3579.
[44] Y. Feng, J.L. Gong, G.M. Zeng, Q.Y. Niu, H.Y. Zhang, C.G. Niu, M. Yan, Adsorption of Cd (II) and Zn (II) from aqueous solutions using magnetic hydroxyapatite nano particles as adsorbents, Chem Eng J., 162(2) (2010) 487–494.
[45] O.M. Freitas, R.J. Martins, C.M. Delerue-Matos, R.A. Boaventura, Removal of Cd (II), Zn (II) and Pb (II) from aqueous solutions by brown marine macro algae: kinetic modeling, J. Hazard. Mater., 153(1) (2008) 493–501.
[46] P.X. Sheng, Y.P. Ting, J.P. Chen, L. Hong, Sorption of lead, copper, cadmium, zinc, and nickel by marine algal biomass: characterization of biosorptive capacity and investigation of mechanisms, J. Colloid Interface Sci., 275(1) (2004) 131–141.
[47] J.H. Van't Hoff, Etudes de dynamique chimique (Vol. 1) (1884) Muller.